Authors copy of Arctic in press; please cite as:

Bauch, D., M. R. v. d. Loeff, N. Andersen, S. Torres-Valdes, K. Bakker, and E. P. Abrahamsen (2011), Origin of freshwater and polynya water in the Arctic Ocean halocline in summer 2007, *Progress in Oceanography*, doi:10.1016/j.pocean.2011.1007.1017

Corresponding Author: Dorothea Bauch

Postal address: Leibniz Institute of Marine Sciences (IFM-GEOMAR), Wischhofstr. 1-3, D-24148-Kiel, Germany

email: dbauch@ifm-geomar.de

Phone: +49 (0)431-6002854

Fax: +49 (0)431-6002961

Keywords:
Arctic Ocean halocline; Surface circulation; Transpolar Drift; Freshwater; Polynyas; Oxygen isotopes

Regional index terms:
Arctic Ocean, Nansen Basin, Amundsen Basin, Makarov Basin, Barents Sea, Laptev Sea

Origin of freshwater and polynya water in the Arctic Ocean halocline in summer 2007

Dorothea Bauch[1], Michiel Rutgers van der Loeff[2], Nils Andersen[3], Sinhue Torres-Valdes[4], Karel Bakker[5], E. Povl Abrahamsen[6]

1 Leibniz Institute of Marine Sciences at University Kiel (IFM-GEOMAR), Wischhofstr. 1-3, Kiel, Germany and Mainz Academy, c/o IFM-GEOMAR
2 Alfred Wegener Institute (AWI), Am Handelshafen 12, D-27570 Bremerhaven
3 Leibniz Laboratory, University Kiel, Max-Eyth-Str. 11-13, 24118 Kiel, Germany
4 Ocean Biogeochemistry and Ecosystems, National Oceanography Centre (NOC), European Way, Southampton, SO14 3ZH, UK
5 NIOZ Royal Netherlands Institute for Sea Research, Postbus 59, 1790 AB Den Burg (Texel), NL
6 British Antarctic Survey, High Cross, Madingley Road, Cambridge, CB3 0ET, UK

Abstract

Extremely low summer sea-ice coverage in the Arctic Ocean in 2007 allowed extensive sampling and a wide quasi-synoptic hydrographic and $\delta^{18}O$ dataset could be collected in the Eurasian Basin and the Makarov Basin up to the Alpha Ridge and the East Siberian continental margin. With the aim of determining the origin of freshwater in the halocline, fractions of river water and sea-ice meltwater in the upper 150 m were quantified by a combination of salinity and $\delta^{18}O$ in the Eurasian Basin. Two methods, applying the preformed phosphate concentration (PO*) and the nitrate-to-phosphate ratio (N/P), were compared to further differentiate the marine fraction into Atlantic and Pacific-derived contributions. While PO*-based assessments systematically underestimate the contribution of Pacific-derived waters, N/P-based calculations overestimate Pacific-derived waters within the Transpolar Drift due to denitrification in bottom sediments at the Laptev Sea continental margin.

Within the Eurasian Basin a west to east oriented front between net melting and production of sea-ice is observed. Outside the Atlantic regime dominated by net sea-ice melting, a pronounced layer influenced by brines released during sea-ice formation is present at about 30 to 50 m water depth with a maximum over the Lomonosov Ridge. The geographically distinct definition of this maximum demonstrates the rapid release and transport of signals from the shelf regions in discrete pulses within the Transpolar Drift.

The ratio of sea-ice derived brine influence and river water is roughly constant within each layer of the Arctic Ocean halocline. The correlation between brine influence and river water reveals two clusters that can be assigned to the two main mechanisms of sea-ice formation within the Arctic Ocean. Over the open ocean or in polynyas at the continental slope where relatively small amounts of river water are found, sea-ice formation results in a linear correlation between brine influence and river water at salinities of about 32 to 34. In coastal polynyas in the shallow regions of the Laptev Sea and southern Kara Sea, sea-ice formation

transports river water into the shelf's bottom layer due to the close proximity to the river mouths. This process therefore results in waters that form a second linear correlation between brine influence and river water at salinities of about 30 to 32. Our study indicates which layers of the Arctic Ocean halocline are primarily influenced by sea-ice formation in coastal polynyas and which layers are primarily influenced by sea-ice formation over the open ocean. Accordingly we use the ratio of sea-ice derived brine influence and river water to link the maximum in brine influence within the Transpolar Drift with a pulse of shelf waters from the Laptev Sea that was likely released in summer 2005.

1. Introduction

The strong vertical gradients in the Arctic Ocean halocline insulate the sea ice cover from the heat in the relatively warm Atlantic waters underneath (Björk and Söderkvist, 2002; Shimada et al., 2005). Below the surface mixed layer there is a strong and cold halocline, which is largely maintained by waters from the shelf seas (Aagaard et al., 1981) as well as convective offshore processes (Steele and Boyd, 1998). About 10 % of the world's river discharge is released onto the Arctic shelf areas. But also large amounts of sea-ice are produced on the shelves by a change from ice-free conditions in summer to freeze-up in autumn and a nearly continuous production of sea-ice in polynyas during winter (Martin and Cavalieri 1989; Bareiss and Görgen, 2005). Between 1979 and 2007, Arctic ice cover declined by ~11 % per decade, and in summer 2007 it was about 37 % less than the average for this period (Comiso et al., 2008). Because of this decline in ice cover, large areas of the ocean especially on the shelves have been free of sea-ice for prolonged periods of time. Climatic changes may have an impact on the freshwater balance of the Arctic Ocean (Dickson et al., 2007; Rabe et al., 2011) and the change in sea-ice cover may specifically influence the occurrence of coastal polynyas and thus, the amount of sea-ice formed there (Willmes et al., 2011). Therefore, in order to further understand possible consequences and feedbacks of the current and future changes, it is of fundamental importance to get a more detailed understanding of the Arctic system and to identify sources of the Arctic Ocean halocline waters with respect to regions and processes of formation.

Lower Halocline Waters, typically characterized by salinities between 34.2 to 34.4, are found in all Arctic basins (Jones and Anderson, 1986). Upper Halocline Water is characterized by a salinity of about 32.8 to 33.2 and a Pacific-derived nutrient maximum (Jones and Anderson, 1986, Weingartner et al., 1998) and is restricted to the Canadian side of the Lomonosov Ridge. Changes in the distribution of Pacific-derived waters and the position of the Transpolar

Drift system are associated with changes in the extent of the Beaufort Gyre, a large anti-cyclonic gyre that dominates the surface circulation of the Canadian Basin. The Transpolar Drift transports surface and halocline waters from the eastern Arctic (at about 180°E) across the pole towards Fram Strait (at about 0°E).

In this study, the origin of waters is identified based on salinity and oxygen isotope values for the upper 150 m of the Arctic Ocean water column in 2007. The fractions of meteoric water, sea-ice meltwater or brine influence as well as marine water are discerned by a combination of salinity and $\delta^{18}O$ in the Eurasian Basin (Bauch et al., 1995). In order to distinguish Atlantic from Pacific sources in the marine fraction, the initial phosphate corrected for mineralization with oxygen (PO*) is used (Ekwurzel et al., 2001). However, since this method systematically underestimates the contribution of Pacific-derived water to the Arctic Ocean halocline mainly because of continuing oxygen exchange with the atmosphere (although restricted below ice cover), the nitrate to phosphate relationship (N/P) is also used (Jones et al., 1998). The N/P method has been successfully applied in the Canadian Basin (Yamamoto-Kawai et al., 2008) and in the Central Arctic Ocean (Jones et al., 1998, 2008), but not along the Siberian continental slope. We therefore apply the N/P-based method but also identify the impact of local denitrification effects on the Siberian shelves, which potentially bias the results. Thus, a combination of the PO*-based and the N/P-based methods are used to constrain the extent of Pacific-derived waters in the Eurasian Arctic and the Transpolar Drift system.

With these methods of water mass analysis, the origin of river water and sea-ice meltwater or formation (i.e. brines) within different layers of the Arctic Ocean halocline are identified. By interpreting the relative contribution from river water and sea-ice processes we are able to identify layers of the Arctic Ocean halocline influenced by sea-ice formation in coastal polynyas versus sea-ice formation over the open ocean. With the ongoing changes in sea-ice coverage in the Arctic Ocean it can be expected that these processes will change in the immediate future and that the relative contributions to the halocline from sea-ice formation in coastal polynyas and over the open ocean will change accordingly.

2. Methods

Water samples were collected during expeditions ARK-XXII/2 onboard *RV Polarstern* (PS07) and NABOS'07 expedition onboard *RV Viktor Buynitskiy* (VB07) in summer 2007 (Fig. 1). On ARK-XXII/2 water samples for stable oxygen isotope analysis were taken with a standard rosette, and a subset of 38 vertical profiles were taken, using an ultra-clean Titanium-rosette with 12 L bottles (De Baar et al., 2008). Accordingly conductivity,

temperature and depth were measured on two CTDs, both Sea Bird electronics and calibrated onboard (Schauer, 2008). Hydrochemical analysis for NO_x (NO_3+NO_2) and PO_4 were conducted in a thermostat-controlled lab container with standard photometric methods using a continuous flow auto analyzer (Technicon TRAACS 800) and dissolved oxygen analyses were conducted with the Winkler Titration method (Schauer, 2008). On NABOS'07 water samples for stable oxygen isotope analysis were taken with a standard rosette and a shipboard SBE19 + CTD was used to record conductivity, temperature and depth vertically every 15-20 cm. All technical details on methods and accuracy of CTD measurements and standard hydrochemical analysis can be found in NABOS'07 cruise technical reports (http://nabos.iarc.uaf.edu/cruise/reports.php). Analytical errors for NO_x are better than ±0.18 µmol/kg and ±0.3 µmol/kg for ARK-XXII/2 and NABOS'07, respectively. For both datasets, analytical errors for PO_4 are better than ±0.015 µmol/kg. Analytical errors for O_2 are ±2.6 µmol/kg and ±0.3 µmol/kg for ARK-XXII/2 and NABOS'07, respectively. Propagated errors for PO* are up to ±0.02 µmol/kg for both datasets.

Oxygen isotopes from all samples collected on PS07 and a subset of samples from VB07 were analyzed at the Leibniz Laboratory (Kiel, Germany) applying the CO_2- water isotope equilibration technique on at least 2 sub-samples on a Finnigan gas bench II unit coupled to a Finnigan DeltaPlusXL. The overall measurement precision for $\delta^{18}O$ analysis is ±0.03‰ or smaller. The $^{18}O/^{16}O$ ratio is given versus V-SMOW in the usual δ-notation (Craig, 1961). A subset of measurements for $\delta^{18}O$ of the eastern sections of VB07 (Fig. 4b) were analyzed at the NERC Isotope Geosciences Laboratory, Keyworth, by equilibration using a VG Isoprep 18, with mass spectrometry performed on a VG Sira 10, yielding an average precision of 0.03‰ on duplicates of these samples. These latter results have been published in combination with barium concentrations by Abrahamsen et al. (2009).

Figures were created using Ocean Data View software (Schlitzer, 2010) and GMT (Wessel and Smith 1998).

3. Results and mass-balance analysis from summer 2007

The upper layers of the Arctic Ocean were close to the freezing point and temperatures underneath rapidly increased between about 50 to 150 m water depth due to the subjacent warm Atlantic layer (Fig. 2). The surface mixed layer over the central Arctic Ocean was between 10 and 30 m thick in summer and separated from underlying waters by a steep salinity gradient (Figs. 3, 4).

Salinity and $\delta^{18}O$ show a first order linear correlation (Fig. 5) due to the mixture of ~0 ‰ $\delta^{18}O$ marine water with significant amounts of isotopically depleted meteoric water. Therefore the distributions of salinity and $\delta^{18}O$ are in first order rather similar. Meteoric water consists of river runoff and local precipitation, with similar isotopic composition due to their common source and is referred to as river water within this study. The deviations from the linear correlation are caused by sea-ice processes. In the southern Eurasian Basin the contributing water masses are river water, sea-ice meltwater and Atlantic-derived waters that can be separated by simple 3-component mass balance calculations (Östlund and Hut, 1984; Fig. 2). The marine source in the northern and eastern Eurasian Basin and in the North American basins (Makarov and Canadian basins) is expected to be a mixture of Atlantic and Pacific-derived waters (Bauch et al., 1995; Ekwurzel et al., 2001; Jones et al., 2008) and a 4-component mass balance has to be applied (Fig. 3, 4). Over the Siberian shelves, the possible effects of local denitrification on the N/P relationship are assessed (see section 3.1). A 3-component, as well as PO*-based and N/P-based 4-component mass balances are applied in the upper 150 m of the water column (section 3.2) that reveal the distribution of river water and net sea-ice processes (section 3.3) as well as the extent of Pacific-derived waters (section 3.4).

3.1 Nitrate to phosphate ratios N/P

Generally nitrate increases or decreases at a ratio of ~16:1 relative to phosphate due to photosynthesis and respiration in the ocean. However, as nutrient-rich Pacific waters enter the Arctic, they are subject to denitrification (Codispoti et al., 1991; Cooper et al., 1999), yielding a N/P signature distinct from that of Atlantic Waters (Jones et al., 1998; Yamamoto-Kawai et al., 2008; Jones et al., 2008). The N/P signatures for stations taken during PS07 and VB07 (Fig. 6) are overall close to the "pure-Atlantic water line" as defined by Jones et al. (1998). Deviations from this correlation line suggest contributions of Pacific-derived waters, that is, values shift towards the "pure-Pacific water line". We define a "pure-Atlantic water line" for our dataset by linear correlation of a subset of station data as $[NO_x] = 16.785*[PO_4] - 1.9126$ (see diamonds and thick red line in Fig. 6) nearly identical to Jones et al. (1998). These stations are in the region of Atlantic inflow of the Arctic Ocean off the continental shelf of the Barents and Kara seas (80-85°N and 30-90°E). We refer to this region as the Atlantic regime since it is not expected to have any contribution of Pacific-derived water.

Some deviations from the "pure-Atlantic water line" are apparent on the Barents Sea shelf (see squares in Fig. 6) and in the Laptev Sea (Fig. 7) where modifications by denitrification

within the sediments may occur. As our analysis relies on NO_x (NO_3+NO_2) and does not include NH_4, the actual value of the N:P ratio might be underestimated, e.g. in high productivity shelf areas where NH_4 concentrations may be high. This in turn would result in the overestimation of the Pacific water contribution (Yamamoto-Kawai et al., 2008). However, NH_4 concentrations over the Laptev Sea have been observed to be low (Nitishinski et al., 2007), and thus the effect on the calculation of Pacific-derived waters is expected to be minor.

Stations from both the central Arctic Ocean (Fig. 7a, open symbols) and the Laptev Sea continental slope (Fig. 7a, closed symbols) show variable deviations from the "pure Atlantic water line" towards the "pure Pacific water line" (Jones et al., 2008; Yamamoto-Kawai et al. 2008). In the central Arctic Ocean deviations are highest at a salinity of about 33 and about 100 m depth (not shown), while towards the surface deviations are seen at lower nutrient concentrations (Fig. 7a, open symbols). At the Laptev Sea continental slope, bottom water samples with salinities of about ~32.5 to 33 have maximal deviations from the "pure Atlantic water line" at low NO_x values. This again indicates denitrification within the sediments, since deviations increase with depth and a Pacific origin can be excluded at 121°E at the Laptev Sea margin. Central Arctic Ocean waters with ~32.5 to 33 salinity and N/P values off the "pure Atlantic water line" (Fig. 7a) probably contain Pacific-derived water, but may also receive part of their elevated N/P signature from Laptev Sea bottom waters if these were transported via the Transpolar Drift.

When comparing stations from the Laptev Sea continental slope at 126 and 131°E (Fig. 7b, open symbols) with the East Siberian Sea continental slope at ~140 to 158°E (Fig. 7b, closed symbols), the propagation of the N/P signal from outer Laptev Sea bottom water can be further inferred. Similar to values found at 121°E (Fig. 7a, closed symbols), deviations from the "pure Atlantic water line" at 126 and 131°E are also maximal at about 30-50 m water depth, nitrate levels of ~5 µmol/kg and salinities of ~32.5 to 33 (Fig. 7b, open symbols). At the East Siberian Sea continental slope (~140 to 158°E) these signals and deviations from the "pure Atlantic water line" (Fig. 7b, closed symbols) are found at about 50 m water depth. At the East Siberian Sea continental slope though, deviations from the "pure Atlantic water line" additionally increase further towards the surface as nitrate values decrease. While the N/P signal found at ~158°E, salinities ~32.5 to 33 and ~50 m water depth may have been propagated from bottom water affected by denitrification in the Laptev Sea (~121°E to ~131°E), the additional N/P signal at ~158°E in low salinity surface waters most likely has a Pacific-derived source.

3.2 Calculation of freshwater fractions and brine-influence in the upper water column

The water mass fractions are calculated using either a 3-component or a 4-component system of mass balance equations based on salinity, $\delta^{18}O$, and PO* or the nitrate to phosphate ratio (N/P).

3.2.1 PO*-based calculation

PO* is based on phosphate and dissolved oxygen and defined as $PO^* = PO_4^{3-} + O_2/175 - 1.95 \cdot \mu molkg^{-1}$ and represents the initial phosphate concentration that accounts for respiration of organic matter according to the Redfield ratios at which dissolved oxygen and phosphate are utilized or released, respectively (Broecker et al., 1985). In deep waters and below a closed sea-ice cover at reduced O_2 atmospheric exchange PO* is assumed to be a quasi-conservative tracer (Ekwurzel et al., 2001). The mass balance is governed by the following equations:

$$f_a + f_p + f_i + f_r = 1 \quad (1)$$

$$f_a S_a + f_p S_p + f_i S_i + f_r S_r = S_{meas} \quad (2)$$

$$f_a O_a + f_p O_p + f_i O_i + f_r O_r = O_{meas} \quad (3)$$

$$f_a PO_a^* + f_p PO_p^* + f_i PO_i^* + f_r PO_r^* = PO_{meas}^* \quad (4)$$

where f_a is the fraction of Atlantic water, f_p the fraction of Pacific-derived water, f_i the fraction of sea ice meltwater, and f_r is the fraction of river water. S, O and PO^* with the corresponding subscripts are the endmember values and measured values of salinity, $\delta^{18}O$ and PO^*. In the Atlantic regime calculated fractions of Pacific-derived water may be strongly negative, because of inaccuracies in end-members and measurements as well as generally non-conservative behavior of dissolved oxygen near the ocean surface. In these cases, Pacific-derived water can be assumed to be absent or negligible and a three-component system of equations is solved instead, only using equations 1-3 with f_p set to zero. Endmember values are given in Table 1, largely following Ekwurzel et al. (2001), but the $\delta^{18}O$ endmember for river water is set to −20 ‰ to reflect average Arctic river water (Bauch et al., 1995). For a detailed discussion on $\delta^{18}O$ of average Arctic Ocean river water refer to Cooper et al. (2008) and Bauch et al. (2010). Uncertainties based on analytical errors are considerably smaller than systematic and conceptual errors arising from limited knowledge of endmember values. Systematic errors in river water and sea-ice meltwater fractions based on uncertainties in endmember salinity and $\delta^{18}O$ data (Tab. 1) remain on average within ±1% for the 3-

component calculations. For the PO*-based 4-component calculation systematic errors due to uncertainties in endmembers are up to about 10% (Ekwurzel et al. 2001). However, systematic and conceptual errors for the PO* methods in the absence of an elevated PO* signal are larger for the Eurasian Basin, and calculations may produce strongly negative numbers in all fractions such that results are not interpretable at all. Although restricted below the ice cover, oxygen exchange with the atmosphere is likely responsible for this conceptual problem in surface waters of the Eurasian basin. Polynyas and leads serve to ventilate Arctic waters despite the ice cover during winter months and oxygen saturation values exceeding 90% have been observed in waters shallower than 50 m (Falkner et al., 2005).

3.2.2 N/P-based calculation

Alternatively we apply the method proposed by Jones et al. (1998), as used in a salinity/$\delta^{18}O$ mass balance by Yamamoto-Kawai et al. (2008). We use the measured NO_x concentration of each sample and derive individual phosphate (P) endmembers for the Pacific and Atlantic fractions from the "pure Atlantic water line" defined for our study ($[NO_x] = 16.785*[PO_4] - 1.9126$; section 3.1) and the "pure Pacific water line" as defined by Jones et al., (2008) ($[NO_x] = 15.314*[PO_4] - 14.395$) for each sample. These endmembers are used in a 4-component mass balance with equations 1-3 and equation 4 is replaced by:

$$f_a P_a + f_p P_p + f_i P_i + f_r P_r = P_{meas} \quad (5)$$

where f_a, f_p, f_i and f_r are as defined above. P with the corresponding subscript is the phosphate value of each endmember or the measured sample. Fixed phosphate endmember values are assigned to river water and sea-ice meltwater (see Tab. 1) in contrast to Jones et al. (2008) and Yamamoto-Kawai et al. (2008), where values of river water and sea-ice meltwater are included within the Atlantic water assignment. Through this alteration the systematic errors are shifted from ignoring the independent impact of river water and sea-ice meltwater on the nutrient balance (as in Jones et al., 1998 and Yamamoto-Kawai et al., 2008) to introducing an independent error to the calculation of river water and sea-ice meltwater fractions. Differences are small, with up to 1% for the river and sea-ice meltwater fractions. For the Pacific water fraction, differences are up to 10%, thus remaining within the uncertainty (~10%) of the method (based on uncertainties in endmember values; see Tab. 1; Yamamoto-Kawai et al., 2008). Due to inaccuracies in end-members and measurements, N/P-based calculations may also produce slightly negative fractions f_p of Pacific-derived waters. These however, remain relatively small also within the Atlantic regime (average f_p are ~-2%, with extreme values up to -10%) and are still within the uncertainty (~10%) of the method (Yamamoto-Kawai et al., 2008). In this respect, the results based on the N/P method are considerably more robust than

the results based on the PO* method. Therefore the presented N/P-based results for f_i and f_r were not replaced with results from the 3-component system when f_p is negative.

3.2.3 Interpretation of calculated fractions

A negative sea-ice meltwater fraction f_i reflects the amount of water removed by sea-ice formation, and the absolute value is proportional to the subsequent addition of brines to the remaining water. In this manuscript we will therefore refer to negative fractions of sea-ice meltwater also as sea-ice derived brine influence or just brine influence. The sea-ice meltwater fraction does not include meltwater from ice formed from river water; this is river water previously transported by ice and is identified by its $\delta^{18}O$ and salinity signature, and it is accounted for in f_r accordingly. All fractions are net values reconstructed from the $\delta^{18}O$, salinity and the nutrient signature of each sample and are the result of time integrated effects on the sample volume over the residence time of the water.

Inventory values of river water and sea-ice meltwater are calculated by integration of each fraction over the upper 150 m of the water column (Fig. 8). Since most of the freshwater is contained in the upper 50 m, the choice of the integration depth is not critical except for the inventory of Pacific-derived water. Uncertainties based on estimates of systematic errors are on average about 10% in absolute inventory values for all applied methods (3-component, PO*-based and N/P-based 4-component).

3.3 Distribution of freshwater and brine-influence in the upper water column

The largest fractions of river water f_r are found in the Makarov Basin near the Lomonosov Ridge, with up to 21 % or 18% based on PO* and N/P calculations, respectively (Fig. 3). In the Laptev Sea the river water fractions f_r reach about 35 % at our southernmost position (Fig. 3; please note that the color scale ends at 20%). The distribution of sea-ice meltwater fractions (positive and negative f_i) roughly exhibits a similar pattern to that of the river water fractions. Positive values of sea-ice meltwater inventories are found in the south-western Eurasian Basin, where river water fractions are quite small (~3%; see Fig. 2). In contrast, in the central and eastern Arctic Ocean river water fractions are large and net sea-ice formation is dominant (see Figs. 3, 4 and compare also inventories in Fig. 8). Only at the surface some additional sea-ice melting is found near the continental slope and in the Makarov Basin. There is a pronounced layer influenced by sea-ice formation present at about 30-50 m water depth east of the New Siberian Islands in the Eurasian Basin and all over the central Arctic Ocean basins. A maximum of this brine influenced layer is observed in the western section over the Lomonosov Ridge (Fig. 3).

3.4 Distribution of Pacific-derived waters in the upper water column

PO*-based fractions of Pacific-derived water f_p are only found in the Makarov Basin (Fig. 3, 4 and compare also inventories in Fig. 8a). In the central Arctic Ocean maximum values are up to 50% at about 75 m depth (Fig. 3), with significant fractions of about 10% still found at about 50 m water depth near the Lomonosov Ridge. N/P-based fractions of Pacific-derived water are considerably higher, with up to ~100% over the Alpha Ridge (Fig. 3), up to ~50% near the East Siberian Sea and significant fractions of ~10% reaching in the Eurasian Basin up to the Gakkel Ridge (at about 86°N and 90°E). Maximum values are located at about 50 m water depth (Fig. 3).

N/P-based f_p of up to ~50% are also found in bottom waters at the continental slope of the central Laptev Sea (Fig. 3b). At this position however, the f_p signal does not originate from Pacific-derived water, but from denitrification in shelf sediments (see 3.1). Further east, near the New Siberian Islands, PO*-based f_p are absent (Fig. 4a), while N/P-based f_p show significant contributions well above 25% within the surface layer. At the continental slope of the East Siberian Sea N/P-based f_p show higher values than PO*-based f_p estimates, and reach farther down to 75 to 100 m water depth (Fig. 4b). At ~50 m water depth the f_p signal originates from the propagation of the apparent f_p signal from the Laptev Sea continental margin (see 3.1).

Since the N/P-based and PO*-based methods yield different ratios of Pacific/Atlantic water, the equations also yield different river water fractions. Thus, if a method overestimated the Pacific fraction (which is lower in salinity) it would underestimate the river water fraction and vice versa. As N/P-based f_p are generally higher compared to PO*-based f_p the N/P-based river water fractions f_r are generally lower compared to PO*-based f_r (Figs. 3, 4). Thus, PO*-based river water inventories (Fig. 8a) in the Makarov Basin at the East Siberian Sea continental slope and over the Alpha Ridge are considerably higher than N/P-based river inventories (Fig. 8b). Sea-ice meltwater fractions and inventories (Fig. 8) remain nearly unaltered when either the N/P-based or PO*-based calculations are applied, since the salinity and $\delta^{18}O$ of the Pacific endmember falls almost exactly on the mixing line between river water and Atlantic endmembers (compare Pacific endmember in Tab. 1 and mixing line in Fig. 5).

4. Discussion

Stable oxygen isotopes of the water in conjunction with salinity have proven to be a useful and reliable tracer to identify and distinguish freshwater sources. Thereby several studies have investigated and described the main features of the Arctic Ocean halocline based on stable isotopes in the Eurasian Basin (e.g. Bauch et al., 1995; Ekwurzel et al., 2001) and the Canadian Basin (e.g. Yamamoto-Kawai et al., 2008). In the following discussion we will evaluate the main features of the freshwater distribution in the Arctic Ocean halocline as observed in our quasi-synoptic dataset from summer 2007 and compare these with earlier $\delta^{18}O$ and PO*-based assessments in the Eurasian Basin by Schlosser et al. (2002) (4.1). The 2007 distribution of Pacific-derived water will be discussed (4.2) and compared with an alkalinity and N/P-based study from 2005, which reaches across the Canadian Basin into the Eurasian Basin (Jones et al., 2008). We will then proceed by focusing on the combined interpretation of f_r and f_i (4.3), that may be used to reveal processes and source areas contributing to the upper layers of the Arctic Ocean halocline in the Eurasian Basin (4.4).

4.1 Freshwater distributions f_r and f_i in 2007

In the northern and western Eurasian Basin there is a front defined by a change between net melting of sea-ice in the region of Atlantic Water inflow and net production of sea-ice concurrent with considerable amounts of river water on the central Arctic side (Figs. 8 and 3) (Bauch et al., 1995; Ekwurzel et al., 2001). The front is mainly oriented from west to east due to the inflow of warm Atlantic Water through Fram Strait and the Barents Sea and the general movement of waters from west to east along the continental slope (Newton et al., 2008). In 2007 the location of this front is approximately 90°E and 85°N over the Gakkel Ridge, where river inventories rapidly increase from about 2 m to 8 m and sea-ice meltwater inventories change from about 1 m to -3 m (see Fig. 8 and Fig. 3). In the region of Atlantic water inflow fractions of river water f_r are correlated to positive values of sea-ice meltwater fractions f_i. This suggests that the small fractions of river water (~3%) present here are transported into this region by ice formed elsewhere in the Arctic (Pfirman et al., 2004) rather than by local runoff. Potential sources could be shelf regions farther east with considerable fractions of river water (Pfirman et al., 1995, 1997). Only the station sampled closest to Franz Josef Land (Fig. 2b) shows river water fractions with small brine influence, whose signal may originate from local runoff.

Our quasi-synoptic dataset from summer 2007 suggests that the spatial and temporal variability is much higher than deduced from earlier assessments. In the 1990s a decline in the extent of the Beaufort Gyre, and thereby a shift of the Transpolar Drift toward the North

American side over the central Arctic Ocean (e.g., Morison et al., 2006), resulted in a thinning of the Arctic Ocean halocline (Steele and Boyd, 1998). Accordingly, the PO*-based assessment by Schlosser et al. (2002) deduced a change in the river water and sea-ice meltwater fractions between parallel sections in the western and eastern Eurasian Basin sampled in 1991 and 1996, respectively. Due to the movement of waters in the Transpolar Drift, the two sections could be linked and variation assumed to be caused by temporal variations and a general thinning of both the amount of river water and the brine influence (neg. f_i) in 1996 relative to 1991 (Schlosser et al., 2002). Our dataset in 2007 indicates that the temporal variability is much higher than assumed by Schlosser et al. (2002): Similar values to those found in 1996, with reduced river water inventories and brine influence are observed in the eastern Eurasian Basin in 2007, while a distinct maximum in river water and brine influence is found over the Lomonosov Ridge close to the pole (Fig. 3a). That is, the 2007 river water inventories of about 12 m and sea-ice meltwater inventories of about -5 m (Fig. 8a) are over the Lomonosov Ridge even more extreme than those observed in 1991 (PO*-based). Since the maximum in brine influence and river water in 2007 is observed in the Transpolar Drift towards Fram Strait (Fig. 3a), but is significantly reduced less than 200 km farther upstream (Fig. 3b), our observations suggest a discrete release of these waters from the shelf and a rather rapid transport in the Transpolar Drift in geographically limited pulses. A freshwater mass balance assessment by Jones et al. (2008) using alkalinity, salinity and N/P also shows two geographically limited maxima close to the Lomonosov Ridge, both correlated to maxima in river water fractions in 2005. Since their 2005 section runs perpendicular, parallel and then perpendicular again relative to the Lomonosov Ridge, and our data indicate that discrete pulses of shelf waters are transported in the Transpolar Drift, we may speculate that these two maxima may represent one or two freshwater pulses from the shelves. Our interpretation that discrete pulses of Siberian shelf waters are transported in the Transpolar Drift is also supported by model simulations. These show the release of river water from the Siberian shelves into the Transpolar Drift in discrete pulses with pronounced seasonal to multi-year variability (Karcher et al., 2006)

4.2 Distribution of Pacific-derived water

Pacific-derived water (f_p) as determined with the PO*-based calculation is observed at the North American side of the Lomonosov Ridge in the Makarov Basin only (see Fig. 8a). Due to some limitations in the PO* calculations (as described above), Pacific-derived water may be underestimated and the N/P method needs to be considered. The PO* method relies on the

assumption of a restricted exchange of oxygen with the atmosphere under the sea-ice cover, which is questionable for the surface mixed layer especially in 2007. Also endmembers for the Pacific component in the PO*-based calculations reflect waters flowing over the Chukchi Sea during winter with relatively high nutrient concentrations (Cooper et al., 1999), and PO*-based calculations may underestimate samples carrying the more nutrient-depleted summer conditions (see Ekwurzel et al., 2001; Yamamoto-Kawai et al., 2008).

The N/P-based estimate accounts for changes caused by photosynthesis and respiration in both marine components, but may produce overestimates in certain areas such as the Siberian continental slope where denitrification creates an apparent f_p signal. This effect is found in Laptev Sea bottom water at a salinity range of about 32.5 to 33 (Fig. 3b) and creates apparent f_p values of up to 50%. This component of Laptev Sea bottom water has a brine signal (neg. fi) of -7 to -10% (Fig. 3b) and spreads eastwards along the continental slope (see section 3.1) and into the Transpolar Drift in accordance with the general surface circulation. In the Transpolar Drift over the Lomonosov Ridge we find water at this salinity range with brine signals of -3 to -4% (neg. fi) somewhat lower compared to Laptev Sea bottom water, while towards the Canadian side, the brine signal disappears (see Fig. 3). Pacific winter water (Upper Halocline Water at S~33.1) is typically also associated with brine production on the Chukchi shelf (Cooper et al., 1997), but due to the decline of the brine signal towards the Canadian side we argue that the brine influence can be regarded primarily as a tracer of Siberian shelf water within this region and the Transpolar Drift. We therefore assume that we may identify the apparent f_p from denitrification at the Laptev Sea continental margin by its brine signal. As the salinity range of Pacific-derived water (~32.7) is identical to this component of brine-enriched Laptev Sea bottom water we estimate the relative contribution of the apparent f_p directly from the dilution of the brine signal to be about 25% over the Lomonosov Ridge. As calculated f_p values are in the same range the entire f_p signal over the Lomonosov Ridge at salinities of about 32.5 to 33 is deduced to be only apparent with origin on the Siberian shelves.

Taking the PO*-based f_p as a lower limit and acknowledging the N/P-based f_p may overestimate Pacific-derived waters, in this case within the Transpolar Drift system, we conclude that overall Pacific-derived water is approximately limited to the position of the Lomonosov Ridge and the Transpolar Drift in 2007.

The freshwater assessment from 2005 by Jones et al. (2008) shows N/P-based Pacific-derived waters on the North American side of the Lomonosov Ridge reaching down to 100 m water depth over the Alpha Ridge as seen also in 2007. Within the Transpolar Drift over the

Lomonosov Ridge the f_p signal of Pacific-derived waters is found at shallower depths, again similar to 2007. Thus, based on our study, we can assume that the N/P-based assessment by Jones et al. (2008) also overestimated Pacific-derived waters in the Transpolar Drift at salinities of about 32.5 to 33 due to the N/P signal from the Siberian shelves to a similar degree.

Recent research support our general conclusions that *i)* Pacific water was limited to the North American side of the Lomonosov Ridge during 2007, and that *ii)* the apparent f_p signal and the concurrent brine signal originates on the Siberian shelves. Using the N/P method, Alkire et al. (2010) found that Pacific-derived waters were nearly absent in the Makarov Basin in spring 2007 and 2008, although they did not take into account any potential contribution of denitrified Siberian shelf waters. Furthermore, Alkire et al. (2010) conclude that meteoric water is likely of Siberian origin in the Makarov Basin in 2007 and 2008. Their N/P based analysis included NH_4 in addition to NO_x (NO_3+NO_2), which improves the accuracy of the method as highly-productive shelf waters may contain high concentrations of NH_4 (Yamamoto-Kawai et al., 2008). However, despite the methodological differences, Alkire et al. (2010) results support our conclusions. While there are indications that Laptev Sea waters are net-denitrifying and NH_4 concentrations are generally low (Nitishinski et al., 2007), no direct measurements are available to confirm or contradict this notion.

4.3 Combined interpretation of f_r and f_i

While fractions of brine influence (neg. f_i) in water parcels may be similar, their salinities can be rather different due to different contributions of river water. If the origin of the brine-enriched layer found in the Arctic Ocean halocline is to be constrained, the signal of brine influence (neg. f_i) together with the corresponding fraction of river water f_r has to be considered. The calculated fractions are net values over the mean residence time of the water. Therefore, both fractions f_i and f_r can be treated as conservative tracers when off the shelves and below the surface mixed layer.

4.3.1 Correlation between f_r and f_i

Brine influence (neg. f_i) and river water (f_r) are roughly linearly correlated (Fig. 9). An approximately constant ratio between inventories of f_i and f_r has been observed before, e.g. in the region of export of Arctic Ocean halocline waters within the western Fram Strait areas (Dodd et al., 2009; Rabe et al., 2009; Meredith et al., 2001; Bauch et al., 1995). However, the correlation between f_i and f_r is absent or weak in the Canadian Basin as indicated by our data over the Alpha Ridge and clearly demonstrated in the freshwater assessment of 2005 by Jones

et al. (2008). This study shows correlated maxima in brine influence and river water close to the Lomonosov Ridge and the Eurasian Basin, but the dominant river water maximum in the central Canadian Basin is accompanied by melting of sea-ice (pos f_i) near the surface, and only at about 50 m water depth it is weakly correlated with brine influence (neg. f_i) (Jones et al., 2008). Sea-ice meltwater fractions and inventories in the Canadian Basin changed considerably and independently from meteoric water between 2003 and 2007 (Yamamoto-Kawai et al., 2009). This independent change further demonstrates the contrast between the Canadian Basin and the Eurasian Basin in respect to the f_i and f_r correlation.

The whole 2007 dataset from the Eurasian and Makarov basins shows a wide range of f_i to f_r ratios, which depend on salinity and corresponding depth level within the halocline (Fig. 9), and on the regional origin too (Fig. 10). However, there are two clusters with similar gradients in f_i versus f_r, but with an offset in f_r values that have salinities of roughly 30-32 and 32-34. We propose that the correlation between brine influence (neg. f_i) and river water (f_r) is caused by sea-ice formation, which transports river water from the surface into layers below the surface mixed layer. Moreover, the division into the two clusters is caused by the two main mechanisms of sea-ice formation within the Arctic Ocean, which can be either in coastal polynyas or in open ocean convection. The salinity range within each cluster reflects slight variations in f_i / f_r ratio and also a varying degree of contribution and thereby dilution by marine waters.

The correlation between f_i and f_r is similar when PO*-based and N/P-based fractions are used, and no significant differences are seen in the two clusters described (compare Fig. 9 a and b).

4.3.2 f_r / f_i ratios at high river water fractions

The linear correlation between brine influence and river water at relatively high f_r values and consequently also relatively low salinity of ~30-32 (Fig. 9, upper grey line), originates from the coastal polynyas on the Eurasian shelves in the Laptev Sea and the Kara Sea, where the river mouths are in close proximity. The so called “Great Siberian Polynya” is a recurrent flaw lead, which is opened by wind forcing mainly in autumn and late winter and is present on the Siberian shelves over ~30 m water depth at the border between the land-fast ice and the pack ice (Zakharov, 1966; Martin and Cavalieri, 1989; Bareiss and Görgen, 2005). On these shallow Siberian shelf regions the fraction of river water f_r and the brine influence (neg. f_i) are correlated in locally formed bottom waters (Bauch et al., 2003, 2005). The coastal polynyas are partly wind-driven and transport river water into the shelf’s bottom layer. Therefore bottom waters from the Kara and Laptev shelf areas with enhanced influence of local polynya activity had a salinity of about 30 (Bauch et al., 2005), compared to a salinity of about 32 in

bottom waters of the Laptev Sea, which had a reduced imprint of local polynya activity (Bauch et al., 2010). The spatial distribution of river water on the Siberian shelves shows strong gradients and interannual variations within the surface layer (Bauch et al., 2009). Salinity and river water fractions may, therefore, vary considerably in the surface layer within the coastal polynyas. Surface waters with a higher river water percentage and lower salinity need more brine influence before they become dense enough to sink to the shelf's bottom layer as is reflected in the roughly linear correlation within the f_i / f_r cluster. Bottom layer salinities on the other hand vary between 30 to 32 only and determine the salinity range of the f_i / f_r cluster formed in the coastal polynyas (Fig. 9, upper grey line).

4.3.3 f_r / f_i ratios at low river water fractions

The linear correlation between brine influence and river water at relatively low levels of f_r with salinities of ~32-34 (Fig. 9, lower cluster, dashed line), originates from sea-ice production over the Arctic Ocean basins or within the polynyas at the continental slope (e.g., at Severnaya Zemlya or in the northern Kara or Barents Sea), where relatively small amounts of river water are found in the surface layer. The Lower Halocline Water (LHW) has salinities between 34.2 to 34.4 (Jones and Anderson, 1986) and is assumed to be formed by similar processes affecting the inflowing Atlantic Water over the Barents Sea shelf (Rudels et al., 2004). Only the upper part of the LHW is therefore included in our discussion (Fig. 9) since we discuss a lower salinity range.

4.4 Geographical analysis of f_r / f_i signatures

Since the general circulation regime in the Arctic Ocean is from west to east along the Eurasian continental slope, the geographical distribution of the f_i to f_r ratios in the southern Eurasian Basin shows the evolution of the different layers of the Arctic Ocean halocline (Fig. 10). The Transpolar Drift transports ice and surface waters from the eastern Makarov Basin in opposite direction across the pole and the propagation and eventual modification of the Arctic Ocean halocline can be investigated along this transport path farther downstream.

4.4.1 Atlantic Regime f_r / f_i

At the Barents Sea and Kara Sea slopes, relatively low river water fractions f_r are found and strong melting of sea-ice is observed at the surface due to the inflow of warm Atlantic Water. Because of the transport of frozen river water as part of the ice, there is also a weak f_i to f_r correlation in surface waters with positive sea-ice meltwater signals (see Fig. 2 and diamonds in Fig. 10). Within the central Eurasian basin river water fractions remain below 10% (Fig. 10, see squares), and there is a correlation between river water and brine influence at salinities

of about 32 to 34 (Fig. 10, 9) attributed to sea-ice formation in open ocean convection or in polynyas at the continental slope of the Barents and northern Kara seas (see 4.3). River runoff increases only at the shelf break of the western Laptev Sea (see triangles in Fig. 10 and Fig. 3).

4.4.2 Laptev Sea f_r / f_i

Waters with constant f_i / f_r at ~32-34 salinities formed west of the Laptev Sea are overlain with waters of constant f_i / f_r at the eastern Laptev Sea margin. These contain considerably higher river water fractions and thereby have lower salinities of ~30-32. We attribute the formation of this second layer to sea-ice formation within the coastal polynyas of the Laptev Sea and also the southern Kara Sea. Since brine-enriched bottom waters with a salinity of about 30 are found in the southern Kara Sea (Bauch et al., 2003), but not at the Kara Sea continental slope (Figs. 10, 8 and compare also Figs. 2b, 3a), a release of brine-enriched bottom water must occur through Vilkitsky Strait directly into the Laptev Sea.

4.4.3 New Siberian Islands and East Siberian Sea f_r / f_i

At the continental slope near the New Siberian Islands (~140°E), relatively high brine (neg f_i) and river fractions f_r are found in surface waters (see closed pink diamonds in Fig. 10 and compare Fig. 4a). Exactly at the slope, a pronounced brine signal is found at about 20 m water depth and 30 salinity (Fig. 4a) similar to the f_i / f_r regime in the south-eastern Laptev Sea bottom waters (see closed pink diamonds and closed triangle in Fig. 10 at f_r of 30% and f_i of -16%). This is in agreement with a bathymetry-steered export of Laptev Sea bottom water at the north-eastern border of the Laptev Sea (Bauch et al., 2009) and is also in accordance with a shift in freshwater storage between the Laptev and the East Siberian seas (Dmitrenko et al., 2008). This layer may also be formed in the East Siberian Sea, but if so the f_i / f_r signature and salinity would be identical to that of the south-eastern Laptev Sea waters, therefore it is not discussed separately here. This relatively high f_r water from the south-eastern Laptev Sea may be deflected northward along the Lomonosov Ridge, but is also found eastward in a rather thin layer at the continental slope of the East Siberian Sea in the Makarov Basin (~158°E, ~30 m water depth; see large open pink diamonds in Fig. 10; Fig. 4b). It can also be seen in N/P signatures (Fig. 7b; see 3.1). Above this thin Laptev Sea-derived layer, a different regime is present, which contains Pacific-derived water fractions of up to about 30% and 75% as determined by the PO*-based and N/P-based methods, respectively. It also contains a strong signal from melting of sea-ice (Figs. 4b, 8, 10). This forms a third f_i / f_r regime, with even lower salinity (~25), but due to addition of sea-ice melting rather than due to additional river water. This layer may be a summer phenomenon only and possibly it may be a feature

restricted to 2007, which was characterized by an exceptionally low summer sea-ice cover and a breakdown of the sea-ice cover especially in the western Canadian Basin (Serreze et al., 2009).

4.4.4 Central Arctic Ocean f_r / f_i

In the central Arctic Ocean f_r / f_i signatures similar to the central Laptev Sea are observed at about 30 to 32 salinity (circles in Fig. 10). We attribute these to a transport of Laptev Sea bottom waters within the Transpolar Drift. A local maximum of this brine-influenced layer is observed in the Transpolar Drift over the Lomonosov Ridge (Fig. 3a; with values of brine maximum and stations highlighted by filled circles in Fig. 10), with values of about -7% in the section perpendicular to the Lomonosov Ridge, which is closer to Fram Strait (Fig. 3a). In the section perpendicular to the Lomonosov Ridge, which is more distant from Fram Strait, fractions of sea-ice meltwater f_i remain at about -4% (Fig. 3b). The geographical limitation of the maximum in brine influence with the direction of the Transpolar Drift indicates the rapid release and transport of this signal from the shelf regions upstream (see 4.1). An outflow of brine-enriched bottom waters from the Laptev Sea has been described at about 30-50 m water depth and about 30 to 32 salinity (Bauch et al., 2009). Also, it has been inferred that the release of shelf waters occurs preferably in years with cyclonic atmospheric wind forcing (Guay et al., 2001; Dmitrenko et al., 2005) and may be rather rapid under certain local wind patterns (Bauch et al., 2011). A pulse of shelf waters was observed at the Laptev Sea continental margin in 2005 related to pronounced off-shore winds, while a similar signal was absent in summer 2006 (Bauch et al., 2011). Annual average current velocities of 2.2 and 2.1 cm/s at about 100 m water depth were estimated from moored instruments at the continental slope east of the Laptev Sea and over the Lomonosov Ridge, respectively (Woodgate et al., 2001). A travel time of 1.8 to 2 years is inferred when applying these velocities for a transport of shelf waters (at slightly shallower depth) over the distance of about 1300 km from the Laptev Sea along the continental slope to the position of the observed maxima in brine influence over the Lomonosov Ridge. This scenario is therefore in agreement with observations, though speculative in respect to vertical velocity variations.

5. Summary and conclusions

In the Eurasian Arctic, a west to east oriented front between net melting of sea-ice and net production of sea-ice is observed concurrent with the occurrence of river water. The Transpolar Drift system is observed at the North American side close to the Lomonosov Ridge. A pronounced layer influenced by brine released during sea-ice formation is present at

about 30-50 m water depth north-east of the Laptev Sea and all over the central Eurasian Basin. A geographically distinct maximum within the Transpolar Drift demonstrates the rapid release and transport of this signal from the Laptev Sea shelf region. It may be speculated that this brine maximum is linked to a release of shelf waters from the Laptev Sea in summer 2005 (Bauch et al., 2011) and transported about 1300 km to the central Arctic Ocean within 2 years in agreement with direct current measurements (Woodgate et al., 2001).

The two clusters seen in the correlation between sea-ice derived brine influence and river water can be assigned to the two main mechanisms of sea-ice formation within the Arctic Ocean. Over the open ocean or polynyas at the continental slope where relatively small amounts of river water are found, sea-ice formation results in a linear correlation between brine influence and river water at salinities of about 32 to 34. In coastal polynyas in the shallow regions of the Laptev and southern Kara seas, sea-ice formation transports river water into the shelf's bottom layer due to the close proximity to river mouths. This process therefore results in waters that form a linear correlation between brine influence and river water at a salinity of about 30 to 32.

With the decline in Arctic sea-ice cover, large areas especially on the shelves are free of sea ice for prolonged periods of time and changes in the seasonal evolution of the coastal polynyas and in the amount of sea-ice formed here are likely. Studies from the south-eastern Laptev Sea already revealed unusually wide and late polynya openings in April 2007 (Willmes et al., 2011), which were not effective in the formation of brine-enriched bottom water (Bauch et al., 2010) usually observed with salinity of about 30 (Bauch et al., 2005). Further studies have to investigate which pattern will be more prominent in the future and how this may affect the Arctic Ocean halocline. With the ongoing climate change the freshwater balance and the fluxes from the Arctic Ocean are also expected to change (Dickson et al., 2007; Rabe et al., 2011). In respect to analyzing freshwater changes and predicting their impact on the structure and stability of the Arctic Ocean halocline our study provides process-oriented information. Our study identifies (1) the layers of the Arctic Ocean halocline influenced by sea-ice formation in coastal polynyas, which are primarily wind-driven and contain larger amounts of river water and (2) the layers of the Arctic Ocean halocline influenced by sea-ice formation over the open ocean, where convection is more dominant. In addition, our study indicates how very rapid signals from the shelves are transported in pulses within the Transpolar Drift system. With the ongoing changes in sea-ice coverage in the Arctic Ocean, it can be expected that the processes of sea-ice formation will change and that

the relative contributions from coastal and open ocean sea-ice formation to the Arctic Ocean halocline will change accordingly.

6. Acknowledgements

This work was funded by the German Research Foundation (DFG) under grant SP526/3.
We are grateful to crews of *RV Polarstern* and *RV Viktor Buynitskiy*, Elena Dobrotina, who did the sampling on VB07, Anna Schmidt and Robert Spielhagen, who did the sampling on PS07, and colleagues for support with sampling and in providing hydrographic data. DB was funded under DFG grant SP526/3. STV and EPA were funded by the Natural Environment Research Council (UK) through the Arctic Synoptic Basin-wide Oceanography (ASBO) IPY consortium grant.

7. References

Aagaard, K., Coachman, L.K., Carmack, E., 1981. On the Halocline of the Arctic Ocean. Deep-Sea Research Part A-Oceanographic Research Papers, 28(6): 529-545.

Abrahamsen, E.P., Meredith, M.P., Falkner, K.K., Torres-Valdes, S., Leng, M.J., Alkire, M.B., Bacon, S., Laxon, S., Polyakov, I., Ivanov, V., Kirillov, S., 2009. Tracer-derived freshwater budget of the Siberian Continental Shelf following the extreme Arctic summer of 2007. Geophysical Research Letters, 36 (L07602), doi:10.1029/2009GL037341.

Alkire, M. B., K. K. Falkner, J. Morison, R. W. Collier, C. K. Guay, R. A. Desiderio, I. G. Rigor, and M. McPhee, 2010. Sensor-based profiles of the NO parameter in the central Arctic and southern Canada Basin: New insights regarding the cold halocline. Deep Sea Research Part I, 57(11), 1432-1443, doi:1410.1016/j.dsr.2010.1407.1011.

Bareiss, J., and K. Görgen, 2005. Spatial and temporal variability of sea ice in the Laptev Sea: Analyses and review of satellite passive-microwave data and model results, 1979 to 2002. Global and Planetary Change, 48, 28-54. doi:10.1016/j.gloplacha.2004.1012.1004.

Bauch, D., Schlosser, P., Fairbanks, R.F., 1995. Freshwater balance and the sources of deep and bottom waters in the Arctic Ocean inferred from the distribution of $H_2{}^{18}O$. Progress in Oceanography, 35, 53-80.

Bauch, D., Erlenkeuser, H., V. Stanovoy, J. Simstich, Spielhagen, R.F., 2003. Freshwater distribution and brine waters in the southern Kara Sea in summer 1999 as depicted by $\delta^{18}O$ results. In: R.Stein, K.F., D. K. Fütterer, E. Galimov (Ed.), Proceedings in Marine Science, Siberian River Run-off in the Kara Sea: Characterization, Quantification, Variability and Environmental Significance.

Bauch, D., Erlenkeuser, H., Andersen, N., 2005. Water mass processes on Arctic shelves as revealed from ^{18}O of H_2O. Global and Planetary Change 48, 165-174, doi:110.1016/j.gloplacha.2004.1012.1011.

Bauch, D., Dmitrenko, I.A., Wegner, C., Hölemann, J., Kirillov, S.A., Timokhov, L.A., Kassens, H., 2009. Exchange of Laptev Sea and Arctic Ocean halocline waters in response to atmospheric forcing. Journal of Geophysical Research, 114 (C05008), doi:10.1029/2008JC005062.

Bauch, D., J. Hölemann, S. Willmes, M. Gröger, A. Novikhin, A. Nikulina, H. Kassens, L. Timokhov, 2010. Changes in distribution of brine waters on the Laptev Sea shelf in 2007. Journal of Geophysical Research, 115, C11008, doi:11010.11029/12010JC006249.

Bauch, D., M. Gröger, I. Dmitrenko, J. Hölemann, S. Kirillov, A. Mackensen, E. Taldenkova, N. Andersen, 2011. Atmospheric controlled freshwater water release at the Laptev Sea Continental margin. *Polar Res.*, 30: 5858 - doi: 10.3402/polar.v30i0.5858.

Björk, G., and J. Söderkvist, 2002. Dependence of the Arctic Ocean ice thickness distribution on the poleward energy flux in the atmosphere, Journal of Geophysical Research, 107(C10), 3173, doi:10.1029/2000JC000723.

Broecker, W.S., Takahashi, T., Takahashi, T., 1985. Sources and flow patterns of deep-ocean waters as deduced from potential temperature, salinity, and initial phosphate concentration. Journal of Geophysical Research, 90: 6925-6939.

Codispoti, L. A., G.E. Friederich, C.M. Sakamoto, L.I. Gordon. 1991. Nutrient cycling and primary production in the marine systems of the Arctic and Antarctic. Journal of Marine Systems, 2.359-84.

Comiso, J.C., Parkinson, C.L., Gersten, R., Stock, L., 2008. Accelerated decline in the Arctic sea ice cover. Geophysical Research Letters, 35, L01703, doi:01710.01029/02007GL031972.

Cooper, L. W., T. E. Whitledge, J. M. Grebmeier, and T. Weingartner, 1997. The nutrient, salinity, and stable isotope composition of Bering and Chukchi seas waters in and near the Bering Strait. Journal of Geophysical Research, 102, 12,563– 512,573.

Cooper, L. W., G. F. Cota, L. R. Pomeroy, J. M. Grebmeier, T. E. Whitledge, 1999. Modification of NO, PO, and NO/PO during flow across the Bering and Chukchi shelves: Implications for use as Arctic water mass tracers. Journal of Geophysical Research, 104, 7827– 7836.

Cooper, L. W., J. W. McClelland, R. M. Holmes, P. A. Raymond, J. J. Gibson, C. K. Guay, B. J. Peterson. 2008. Flow-weighted values of runoff tracers ($\delta^{18}O$, DOC, Ba, alkalinity) from the six largest Arctic rivers. Geophysical Research Letters, 35(18), L18606, doi:10.1029/2008GL035007.

Craig, H., 1961. Standard for reporting concentrations of Deuterium and Oxygen-18 in natural waters. Science 133, 1833-1834.

De Baar, H.J.W. et al., 2008. Titan: A new facility for ultraclean sampling of trace elements and isotopes in the deep oceans in the international Geotraces program. Marine Chemistry, 111(1-2): 4-21.

Dickson, R., B. Rudels, S. Dye, M. Karcher, J. Meincke, I. Yashayaev, 2007. Current estimates of freshwater flux through Arctic and subarctic seas. Progress in Oceanography, 73(3-4), 210-230.

Dmitrenko, I.A., Kirillov, S.A., Eicken, H., Markova, N., 2005. Wind-driven summer surface hydrography of the eastern Siberian shelf. Geophysical Research Letters 32, L14613, doi:14610.11029/12005GL023022.

Dmitrenko, I.A., Kirillov, S.A., Tremblay, L.B., 2008. The long-term and interannual variability of summer fresh water storage over the eastern Siberian shelf: Implication for climatic change. Journal of Geophysical Research, 113, C03007, doi:03010.01029/02007JC004304.

Dodd, P.A., Heywood, K.J., Meredith, M.P., Naveira-Garabato, A.C., Marca, A.D., & Falkner, K.K., 2009. Sources and fate of freshwater exported in the East Greenland Current. Geophysical Research Letters, 36, L19608, doi:19610.11029/12009GL039663.

Ekwurzel, B., Schlosser, P., Mortlock, R.A., Fairbanks, R.G., Swift, J.H., 2001. River runoff, sea ice meltwater, and Pacific water distribution and mean residence times in the Arctic Ocean. Journal of Geophysical Research, 106(C5): 9075-9092.

Falkner, K. K., M. Steele, R. A. Woodgate, J. H. Swift, K. Aagaard, and J. Morison, 2005. Dissolved oxygen extrema in the Arctic Ocean halocline from the North Pole to the Lincoln Sea. Deep-Sea Research, 52, 1138-1154.

Guay, C.K., Falkner, K.K., Muench, R.D., Mensch, M., Frank, M., Bayer, R., 2001. Wind-driven transport pathways for Eurasian Arctic river discharge. Journal of Geophysical Research, 106 (C6), 11,469-411,480.

Jones, E., and L. Anderson, 1986. On the origin of the chemical properties of the Arctic Ocean Halocline. Journal of Geophysical Research, 91(C9), 10,759-710,767.

Jones, E., Anderson, L., Swift, J., 1998. Distribution of Atlantic and Pacific water in the upper Arctic Ocean: Implications for circulation. Geophysical Research Letters, 25, 765-768.

Jones, E.P., L. G. Anderson, S. Jutterström, L. Mintrop, J. H. Swift, 2008. Pacific freshwater, river water and sea ice meltwater across Arctic Ocean basins: Results from the 2005 Beringia Expedition. Journal of Geophysical Research, 113, C08012, doi:08010.01029/02007JC004124.

Karcher, M., Gerdes, R., Kauker, F., 2006. Modeling of $\delta^{18}O$ and ^{99}Tc dispersion in Arctic and subarctic seas. ASOF Newsletter, Issue No 5, April 2006. Accessible under: http://epic.awi.de/epic/Main?static=yes&page=abstract&entry_dn=Kar2006d

Nitishinsky, M., L. G. Anderson, and J. A. Hölemann, 2007. Inorganic carbon and nutrient fluxes on the Arctic Shelf. Continental Shelf Research 27, 1584–1599, doi:1510.1016/j.csr.2007.1501.1019.

Martin, S., and D. J. Cavalieri, 1989. Contributions of the Siberian Shelf polynyas to the Arctic Ocean intermediate and deep water. Journal of Geophysical Research, 94(C9), 12,725-712,738.

Meredith, M., Heywood, K., Dennis, P., Goldson, L., White, R., Fahrbach, E., Schauer, U., Østerhus, S., 2001. Freshwater fluxes through the western Fram Strait. Geophysical Research Letters, 28, 1615-1618.

Morison, J., M. Steele, T. Kikuchi, K. Falkner, W. Smethie, 2006. Relaxation of central Arctic Ocean hydrography to pre-1990s climatology. Geophysical Research Letters, 33, L17604, doi:17610.11029/12006GL026826.

Newton, R., Schlosser, P., Martinson, D.G., Maslowski, W., 2008. Freshwater distribution in the Arctic Ocean: Simulation with a high resolution model and model-data comparison. Journal of Geophysical Research, 113 (C05024), doi:10.1029/2007JC004111.

Östlund, H.G. and Hut, G., 1984. Arctic Ocean Water Mass Balance from Isotope Data. Journal of Geophysical Research, 89(NC4): 6373-6381.

Pfirman, S., Haxby, W., Eicken, H., Jeffries, M., Bauch, D., 2004. Drifting Arctic sea ice archives changes in ocean surface conditions. Geophysical Research Letters, 31, L19401, doi:19410.11029/12004GL020666.

Pfirman, S., H. Eiken, D. Bauch, W.F. Weeks, 1995. The Potential Transport of Pollutants by Arctic Sea Ice. The Science of the Total Environment, 159, 129-146.

Pfirman, S.L., Colony, R., Nürnberg, D., H., Eiken, I., Rigor, 1997. Reconstructing the origin and trajectory of drifting Arctic sea ice. Geophysical Research Letters, 102, 12575-12586.

Rabe, B., U. Schauer, A. Mackensen, M. Karcher, E. Hansen, A. Beszczynska-Möller, 2009. Freshwater components and transports in the Fram Strait – recent observations and changes since the late 1990s. Ocean Science, www.ocean-sci.net/5/219/2009/, 5, 219–233.

Rabe, B., M. Karcher, U. Schauer, A. J. M. Toole, R. A. Krishfeld, S. Pisarev, F. Kauker, R. Gerdes, T. Kikuchi. 2011. An assessment of Arctic Ocean freshwater content changes from the 1990s to the 2006-2008 period. Deep-Sea Research Part I, 58(2), 173-185, doi: 10.1016/j.dsr.2010.12.002.

Rudels, B., Jones, E.P., Schauer, U. Eriksson, P., 2004. Atlantic sources of the Arctic Ocean surface and halocline waters. Polar Research, 23(2), 181-208.

Schauer, U., 2008. The expedition ARKTIS-XXII/2 of the research vessel "Polarstern" in 2007. Berichte zur Polar- und Meeresforschung - Reports on polar and marine research, 579: 271pp.

Schlitzer, R., 2010. Ocean Data View, http://odv.awi.de.

Schlosser, P., R. Newton, B. Ekwurzel, S. Khatiwala, R. Mortlock, R. F. Fairbanks, 2002. Decrease of river-runoff in the upper waters of the Eurasian Basin, Arctic Ocean, between 1991 and 1996: Evidence from δ18O data. Geophysical Research Letters, 29(9, 1289), doi.: 10.1029/2001GLO13135.

Serreze, M. C., A. P. Barrett, J. C. Stroeve, D. N. Kindig, M. M. Holland, 2009. The emergence of surface-based Arctic amplification. The Cryosphere, 3, 11-19, doi:10.5194/tc-5193-5111-2009.

Shimada, K., M. Itoh, and F. M. S. Nishino, E. Carmack, A. Proshutinsky, 2005. Halocline structure in the Canada Basin of the Arctic Ocean. Geophysical Research Letters, 32, L03605, doi:03610.01029/02004GL021358.

Steele, M., and Boyd, T., 1998. Retreat of the cold halocline layer in the Arctic Ocean. Journal of Geophysical Research, 103 (C5), 10,419-410,435.

Weingartner, T.J., Cavalieri, D.J., Aagaard, K., Sasaki, Y., 1998. Circulation, dense water formation, and outflow on the northeast Chukchi shelf. Journal of Geophysical Research, 103(C4): 7647-7661, doi:10.1029/98JC00374.

Wessel, P., and W. H. F. Smith, 1998. New improved version of the Generic Mapping Tools released. EOS Trans. AGU, 79, 579.

Willmes, S., S. Adams, D. Schroeder, G. Heinemann. 2011. Spatiotemporal variability of sea-ice coverage, polynya dynamics and ice production in the Laptev Sea between 1979 and 2008. Polar Research, 30, 5971, doi: 5910.3402/polar.v5930i5970.5971.

Woodgate, R. A., K. Aagaard, R. D. Muench, J. Gunn, G. Björk, B. Rudels, A. T. Roach, U. Schauer, 2001. The Arctic Ocean Boundary Current along the Eurasian slope and the adjacent Lomonosov Ridge: Water mass properties, transports and transformations from moored instruments. Deep-Sea Research I, 48, 1757-1792.

Yamamoto-Kawai, M., F. A. McLaughlin, E. C. Carmack, S. Nishino, K. Shimada, 2008. Freshwater budget of the Canada Basin, Arctic Ocean, from salinity, $\delta^{18}O$, and nutrients. Journal of Geophysical Research, 113(C01007), doi:10.1029/2006JC003858.

Yamamoto-Kawai, M., F. A. McLaughlin, E. C. Carmack, S. Nishino, K. Shimada, and N. Kurita, 2009. Surface freshening of the Canada Basin, 2003–2007: River runoff versus sea ice meltwater. Journal of Geophysical Research, 114(C00A05), doi: 10.1029/2008JC005000.

Zakharov, V.F., 1966. The role of flaw leads off the edge of fast ice in the hydrological and ice regime of the Laptev Sea. Oceanology 6 (1), 815–821.

8. List of Tables:

			PO*-based	**N/P-based**
endmember	salinity	$\delta^{18}O$ (‰)	PO* ($\mu mol \cdot kg^{-1}$)	PO_4 ($\mu mol \cdot kg^{-1}$)
Atlantic Water (f_a)	34.92(5)	0.3(1)	0.70(5)	$0.0596*[NO_x] + 0.1139 \pm 0.02$
river water (f_r)	0	-20(1)	0.1(1)	0.1(1)
sea-ice meltwater (f_i)	4(1)	surface[a]+2.6(1)	0.4(1)	0.4(1)
Pacific water (f_p)	32.7(2)	-1.1(2)	2.4(3)	$0.0653*[NO_x] + 0.9400 \pm 0.02$

Tab. 1: Endmember values used for the three component (bold outline) and PO*-based and N/P-based four component mass-balance calculations. Numbers given in parentheses are the estimated uncertainties within the last digit in our knowledge of each endmember value. Analytical errors are all considerably smaller. [a] Average Arctic surface water $\delta^{18}O$ of -2‰ was used and within the southern Eurasian Basin the surface value of each station was applied. For further explanation see text.

9. List of Figures

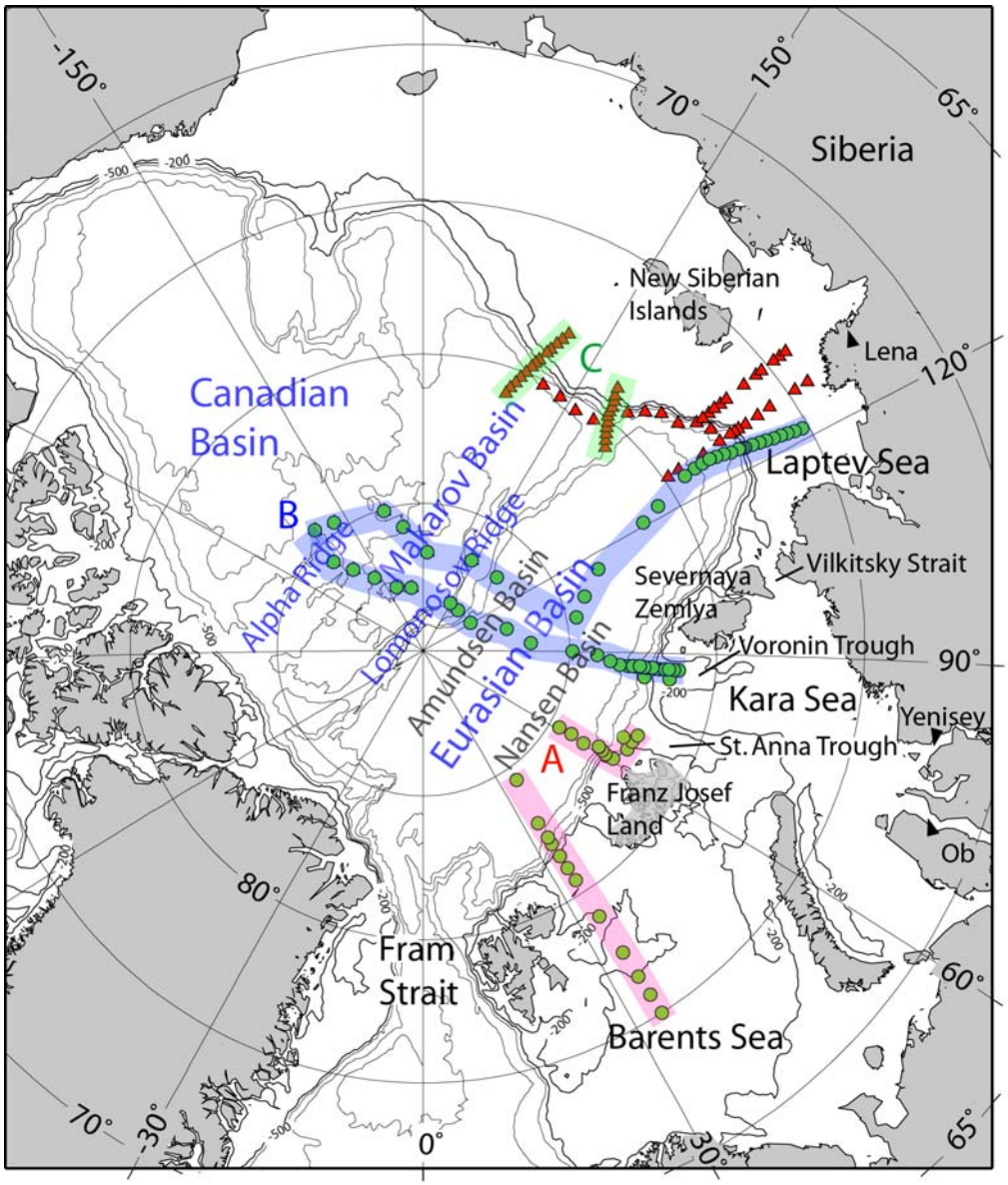

Fig. 1: Map of the Arctic Ocean with geographical distribution of stations with $\delta^{18}O$ data taken during expeditions PS07 (circles) and VB07 (triangles) in 2007. Also indicated are the positions of the sections A-C shown in Figs. 2-4, respectively.

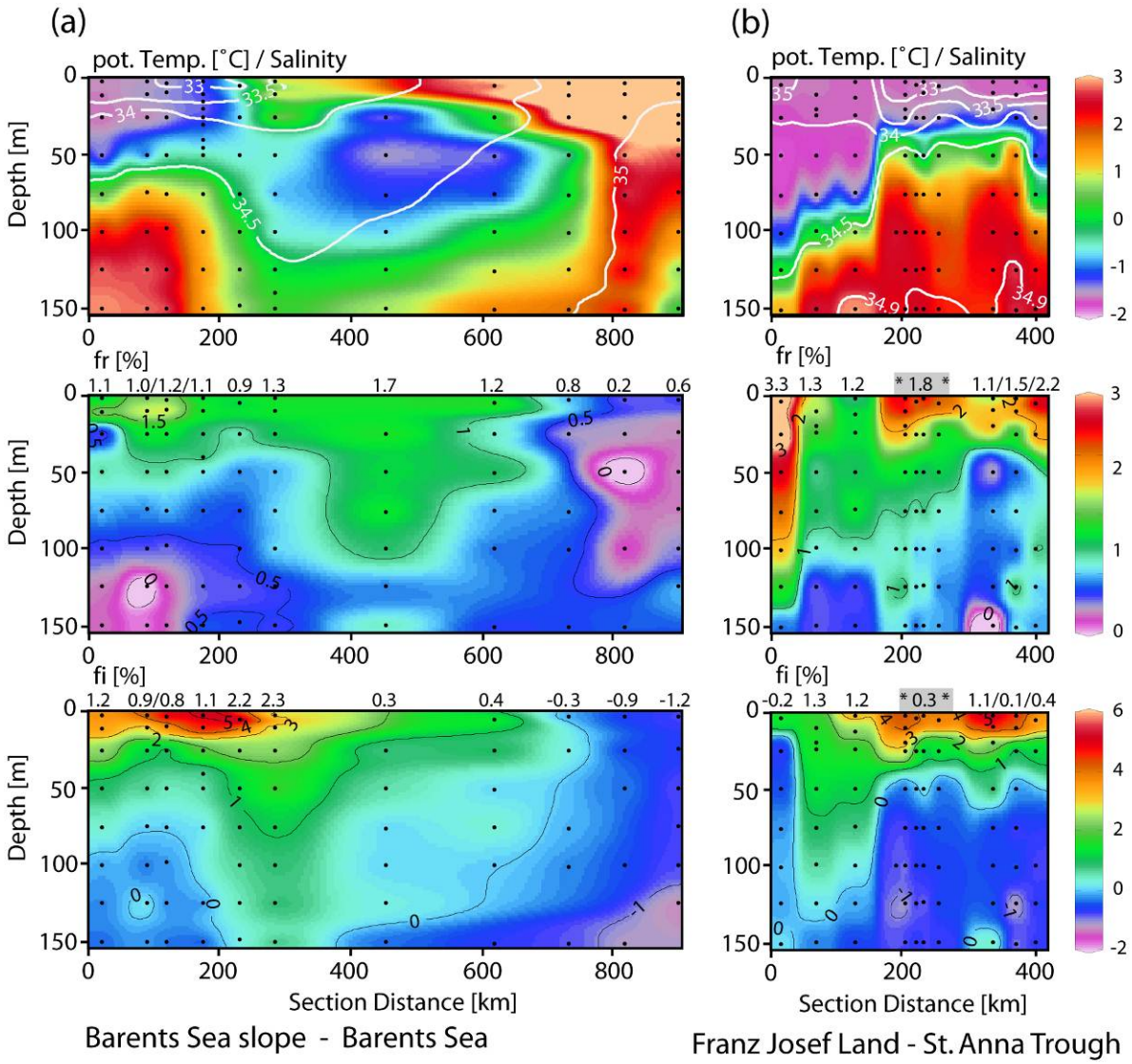

Fig. 2: Hydrographic and derived parameters within the upper 150 m water depth on sections A as indicated in Fig. 1 from (a) the Atlantic regime across the continental margin at the Barents Sea at ~35°E and (b) Franz Josef Land/St. Anna Trough at ~60 to 69°E. In the upper panels color shading show potential temperatures and salinities are superimposed in white contour lines. Middle panels show fractions of river water f_r and lower panels show fractions of sea-ice meltwater f_i based on the 3-component mass balance. The small dots within the sections show the position of the samples in the water column. Inventory values for the upper 150 m are given as pure river water or sea-ice meltwater in m on top of each station or average of stations between asterisks and highlighted by gray shading.

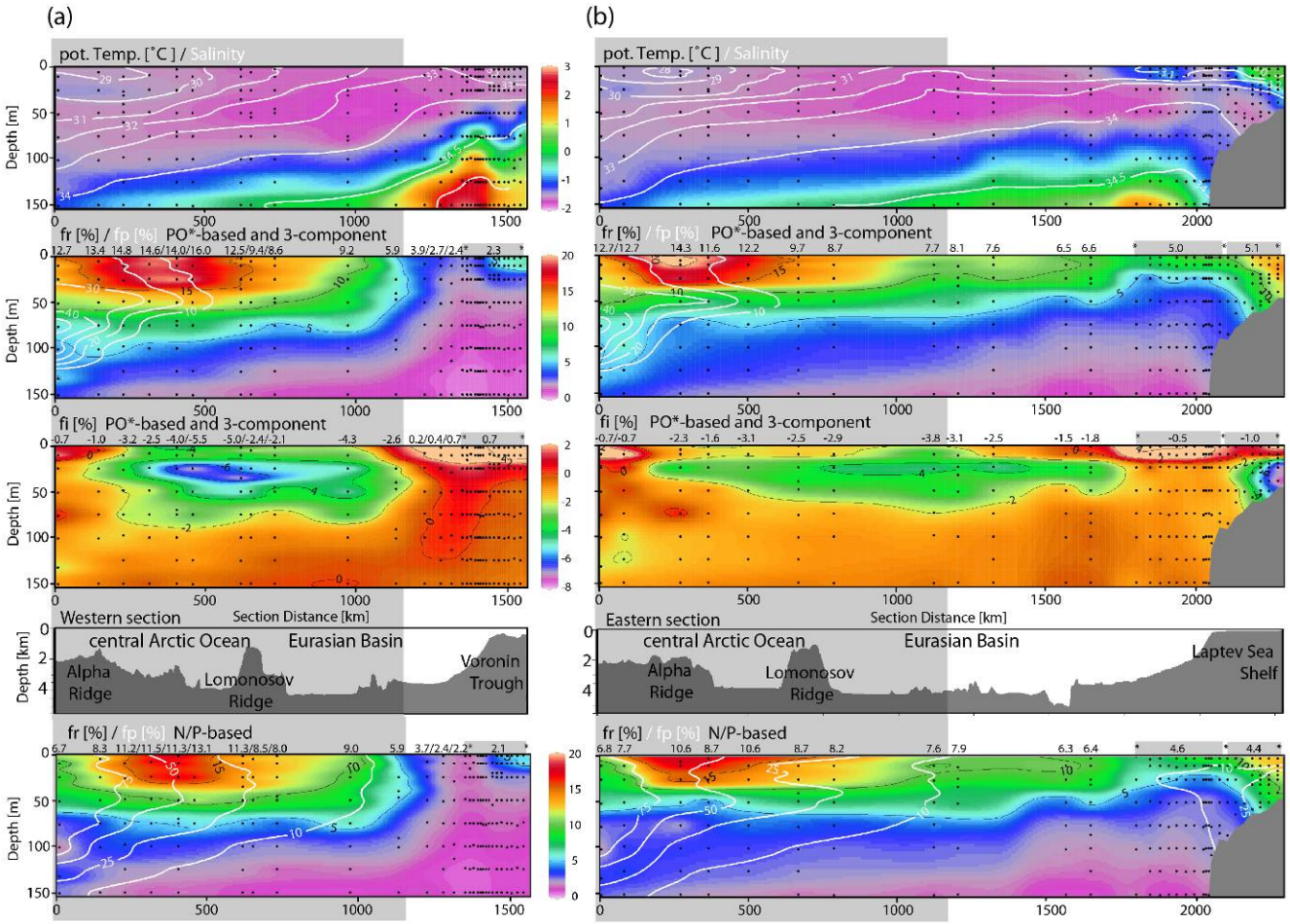

Fig. 3: Hydrographic and derived parameters within the upper 150 m water depth on sections B as indicated in Fig. 1 from (a) the central Arctic Ocean across the Eurasian basin towards Voronin Trough and (b) towards the Laptev Sea. The parallel parts of the sections are highlighted by gray shading. In the upper panels color shading show potential temperatures and salinities are superimposed in white contour lines. Middle panels show PO*-based fractions of river water f_r and sea-ice meltwater f_i (3-component when PO*-based f_p is absent), with fractions of Pacific-derived water f_p shown in white contour lines. In the lower panels N/P-based fractions are shown for f_r and f_p. The small dots within the sections show the position of the samples in the water column. Inventory values in the upper 150 m (or bottom depth) are given as pure river water or sea-ice meltwater in m on top of each station or as average of stations between asterisks and highlighted by gray shading.

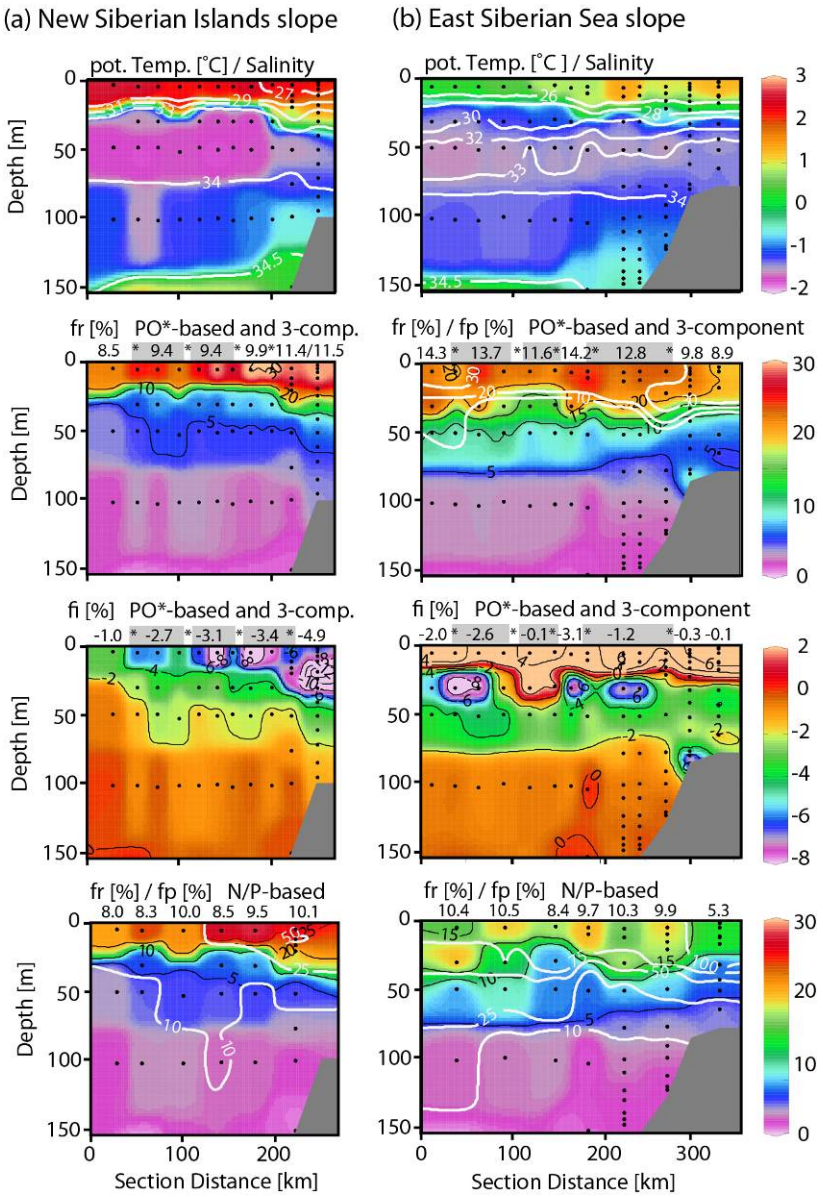

Fig. 4: Hydrographic and derived parameters within the upper 150 m water depth on two sections (marked C in Fig. 1) from the Makarov Basin across the continental margin of (a) the New Siberian Islands at ~141°E and (b) the East Siberian Sea at ~158°E. In the upper panels color shading show potential temperatures and salinities are superimposed in white contour lines. Middle panels show fractions of river water f_r and sea-ice meltwater f_i. When present, fractions of Pacific-derived water f_p are shown in white contour lines. PO*-based fractions (middle rows; 3-component when PO*-based f_p is absent) and N/P-based fractions f_r and f_p are shown (lower row). The small dots within the sections show the position of the samples in the water column. Inventory values for the upper 150 m (or bottom depth) are given as pure river water or sea-ice meltwater in m on top of each station or as average of stations between asterisks and highlighted by gray shading.

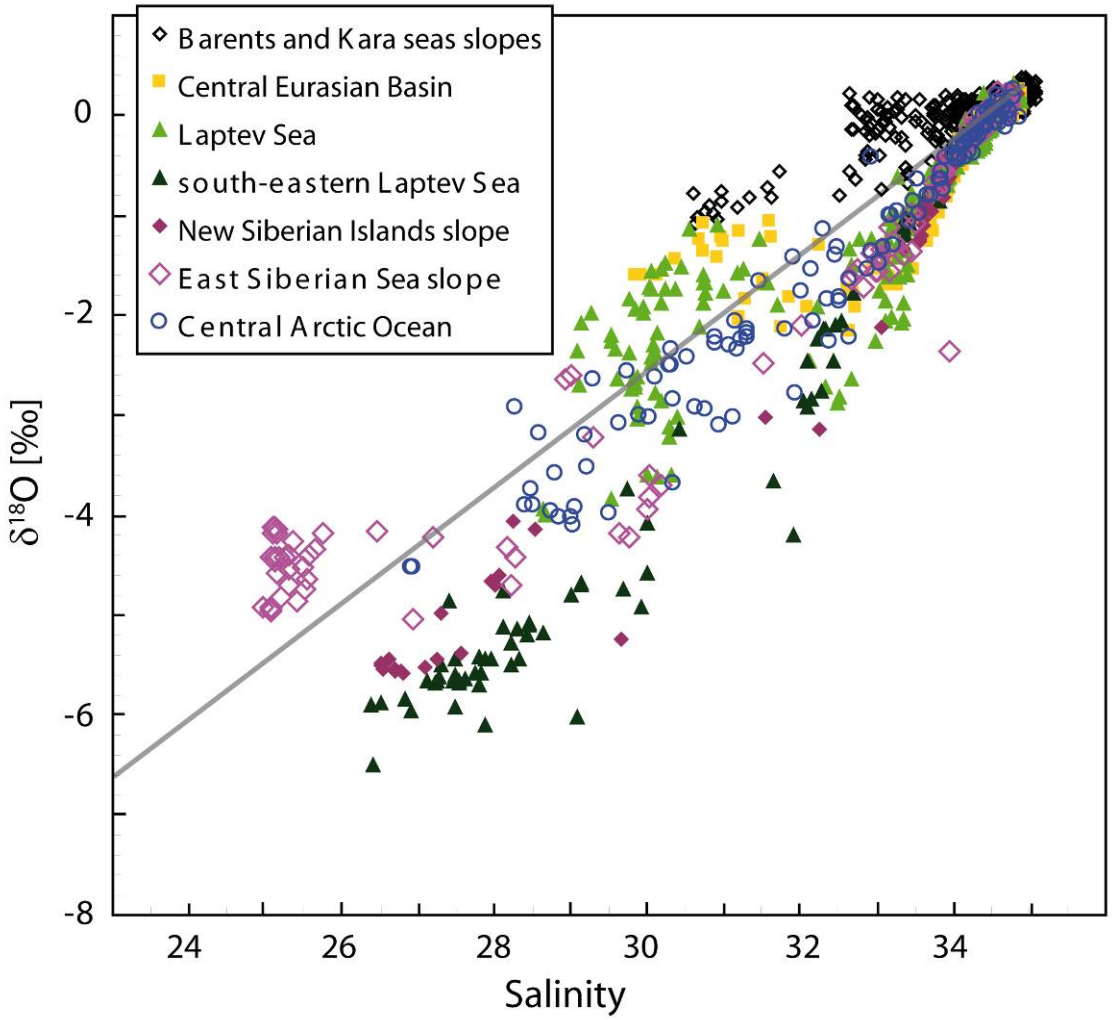

Fig. 5: Property plot of $\delta^{18}O$ values versus salinity for the upper 150 m of the Arctic Ocean water column in 2007. The geographical distribution of each sample is indicated by different symbols according to the legend and is also shown in the map included in Fig. 10. Also indicated is the mixing line between the endmember values of Atlantic Water in the Arctic Ocean and average river water as used in the mass balance calculations. For further explanation see text.

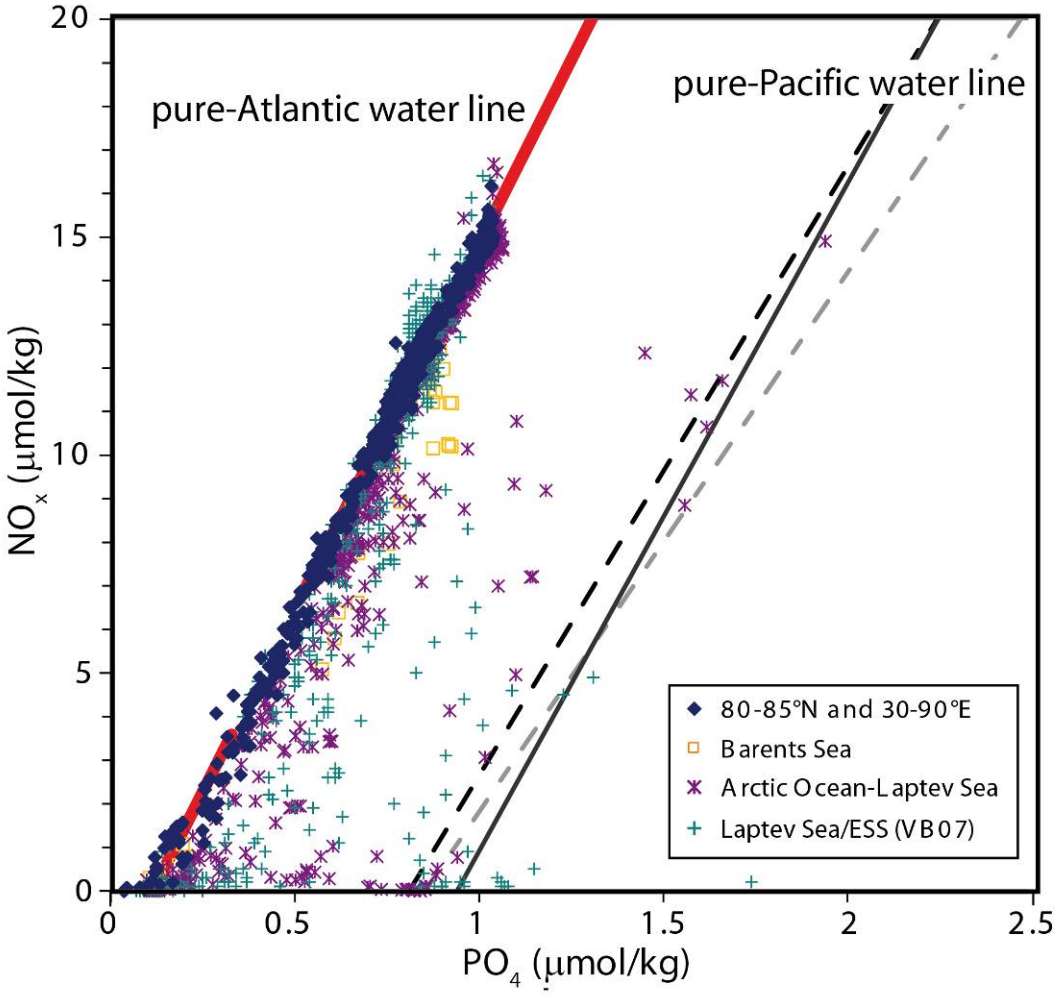

Fig. 6: NO_x (NO_2+NO_3) versus PO_4 for stations taken during PS07 and VB07. The "pure-Atlantic water line" (thick red line) is defined by linear correlation of all station data in the Atlantic regime between 80-85°N and 30-90°E (diamonds) as $[NO_x] = 16.785*[PO_4] -1.9126$. Also indicated are the "pure-Pacific water line" as defined by Jones et al. 1998 (gray stippled line), Yamamoto-Kawai et al. 2008 (black stippled line) and Jones et al., 2008 (solid black line).

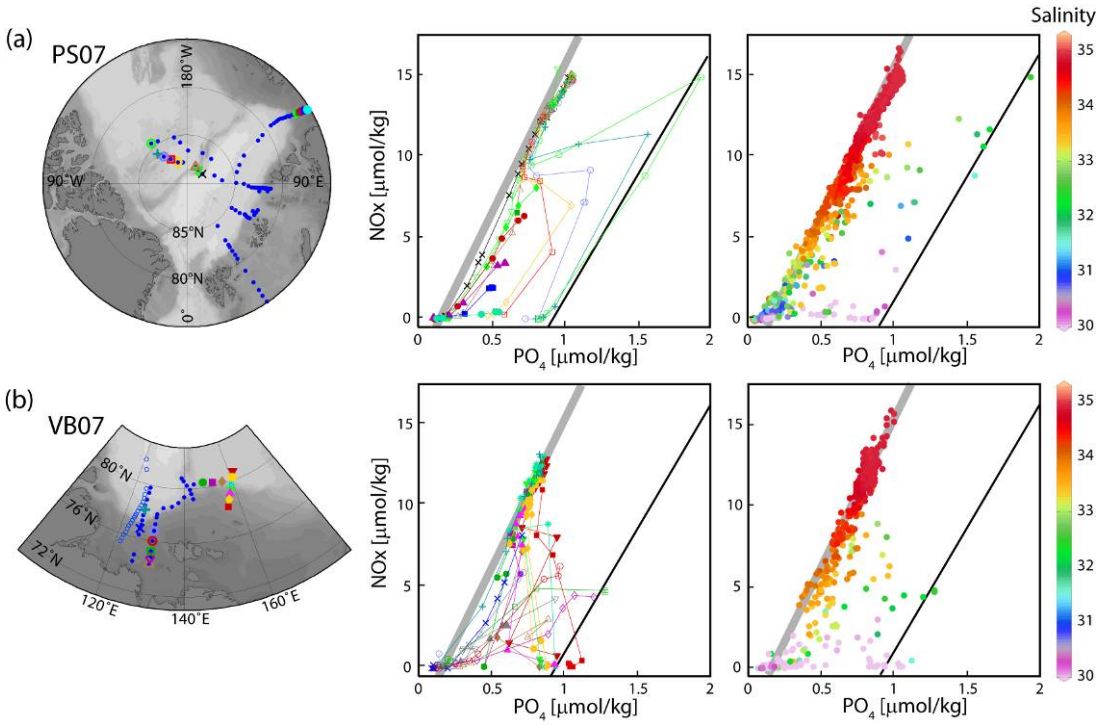

Fig. 7: NO_x (NO_2+NO_3) versus PO_4 for stations taken during (a) PS07 and (b) VB07. Middle panel in (a) shows selected stations from PS07 in the central Arctic Ocean (open symbols as indicated in map) and the Laptev Sea continental slope (closed symbols as indicated in map). Middle panel in (b) shows selected stations from VB07 at the Laptev Sea continental slope (open symbols as indicated in map) and the East Siberian Sea continental slope (closed symbols as indicated in map; for orientation open dots indicate also PS07 station positions). Right hand side panels show scatter plots for all samples from each expedition with salinity indicated by coloring. Also indicated are the "pure Atlantic water line" (thick gray line, as defined in Fig. 6) and the "pure Pacific water line" (black line, as defined by Jones et al., 2008). For further explanation see text.

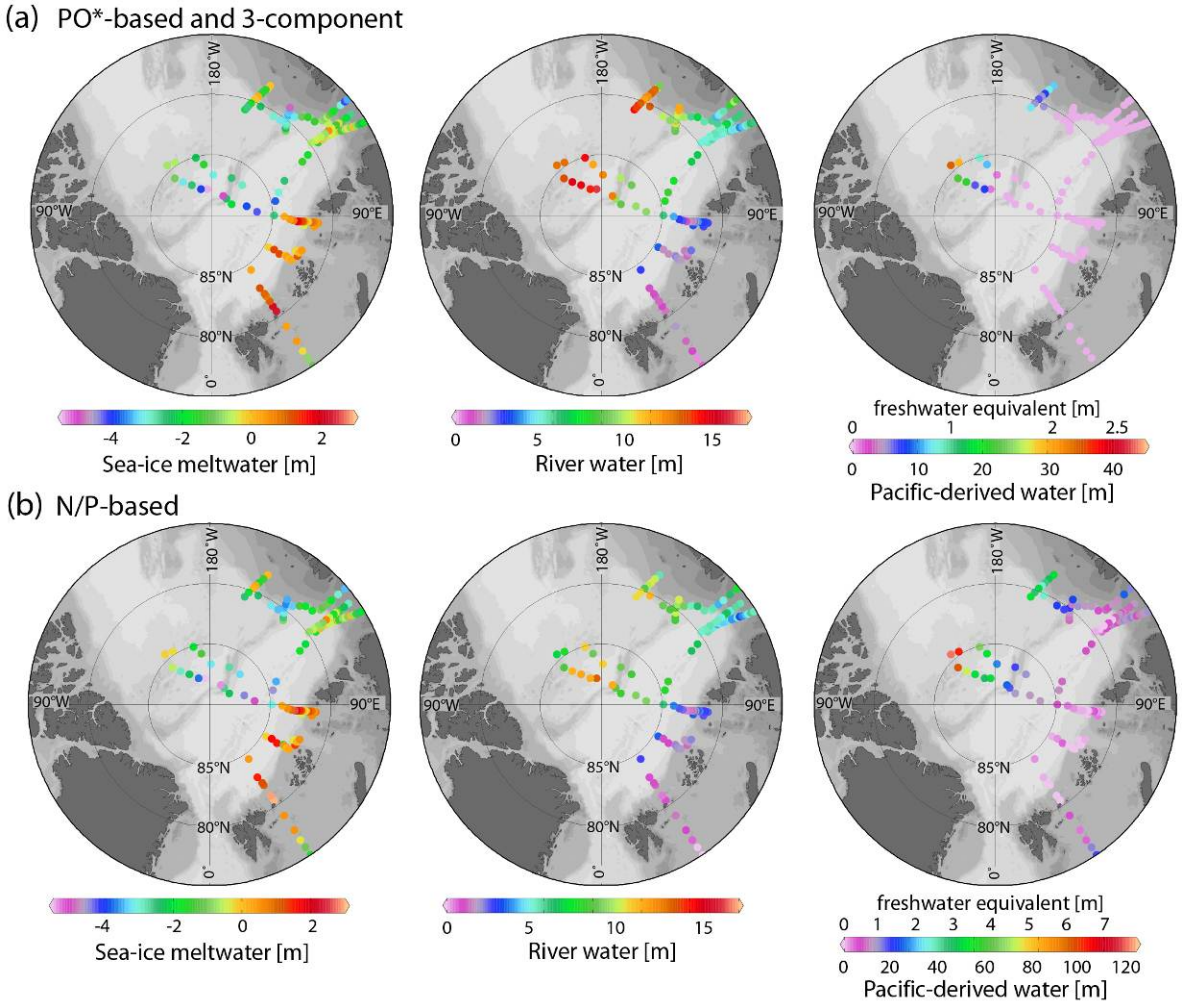

Fig. 8: Map of the Arctic Ocean with geographical distribution of inventory values of the upper 150 m for stations in 2007. Inventory values are a) PO*-based and 3-component and b) N/P-based. Inventory values are given as pure river water, sea-ice meltwater and Pacific-derived water in m. The color bar for Pacific-derived water also shows the freshwater equivalent relative to S=34.92 (salinity of Atlantic endmember). Note that scales for Pacific-derived inventory N/P-based and PO*-based are different.

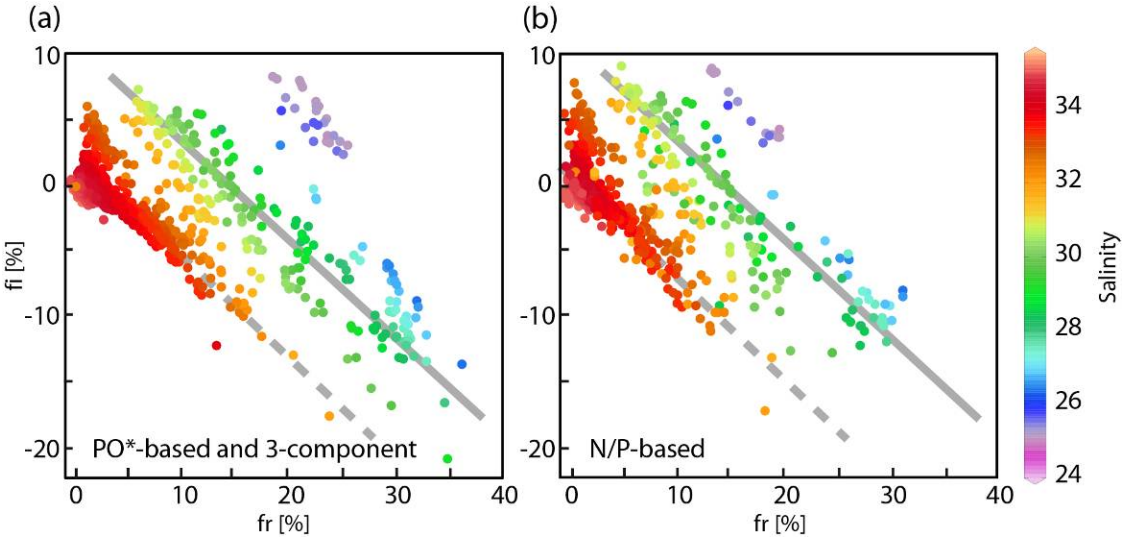

Fig. 9: Property plots of sea-ice meltwater fraction f_i versus river water fraction f_r for the upper 150 m of the water column in the Arctic Ocean in 2007. The corresponding salinity of each sample is indicated by colored dots. Fractions are calculated a) PO*-based and 3-component and b) N/P-based. For further explanation see text. The dashed and solid gray lines mark the clusters at salinities of about 32-34 and 30-32, respectively.

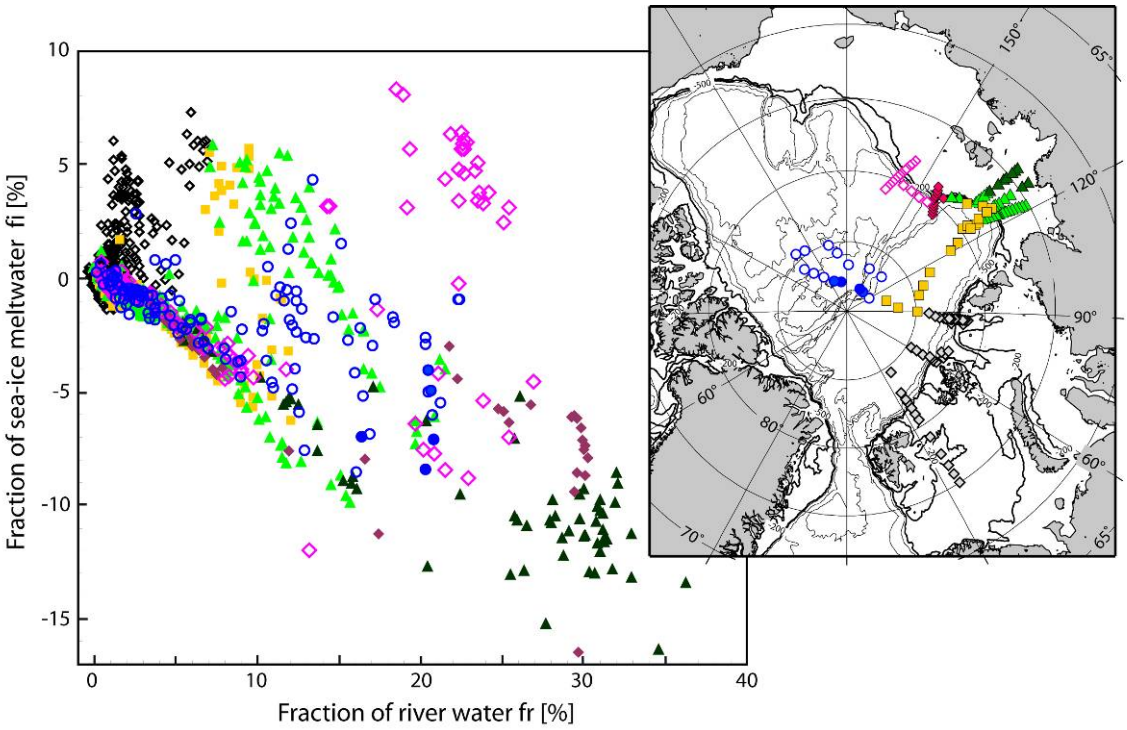

Fig. 10: Property plot of sea-ice meltwater fraction f_i versus river water fraction f_r (PO*-based and 3-component) for the upper 150 m of the water column in the Arctic Ocean in 2007. The geographical distribution of each sample is indicated by different symbols as shown in the map. Within the stations in the central Arctic Ocean (open circles) the maximum of the brine layer over the Lomonosov Ridge is highlighted by filled symbols.